

X-Ray Thomson-Scattering Measurements of Density and Temperature in Shock-Compressed Beryllium

H. J. Lee,¹ P. Neumayer,² J. Castor,² T. Döppner,² R. W. Falcone,¹ C. Fortmann,³ B. A. Hammel,² A. L. Kritcher,^{1,2} O. L. Landen,² R. W. Lee,² D. D. Meyerhofer,⁴ D. H. Munro,² R. Redmer,³ S. P. Regan,⁴ S. Weber,² and S. H. Glenzer²

¹University of California, Berkeley, California 94720, USA

²Lawrence Livermore National Laboratory, Livermore, California 94551, USA

³Institut für Physik, Universität Rostock, D-18051 Rostock, Germany

⁴Laboratory for Laser Energetics, Rochester, New York 14623, USA

(Received 4 September 2008; published 16 March 2009)

We present the first x-ray scattering measurements of the state of compression and heating in laser irradiated solid beryllium. The scattered spectra at two different angles show Compton and plasmon features indicating a dense Fermi-degenerate plasma state with a Fermi energy above 30 eV and with temperatures in the range of 10–15 eV. These measurements indicate compression by a factor of 3 in agreement with Hugoniot data and detailed radiation-hydrodynamic modeling.

DOI: 10.1103/PhysRevLett.102.115001

PACS numbers: 52.70.La, 52.25.Os, 52.35.Fp, 52.50.Jm

Measurements of the conditions of compressed matter comprise a key scientific activity important for the investigation of many physical and chemical phenomena. At pressures above 1 Mbar, high-energy density physics conditions are accessed where phase transitions [1], quantum fluids [2], and conditions of Jovian planets [3] have been studied. Higher pressure conditions above 100 Mbar have been predicted for inertial confinement fusion (ICF) experiments [4,5], where powerful laser or particle beams will be used to heat and compress matter to approach densities of 1000 g/cc. In these regimes, direct and accurate measurements of thermodynamic and physical properties are of great interest to test dense plasma modeling and to address fundamental physics questions such as the equation of state and the structure of dense matter.

Powerful laser-produced x-ray sources have been developed for probing dense matter. They produce quasimonochromatic line radiation capable of penetrating through dense and compressed materials at solid density and above [6,7]. Both thermal Ly- α and He- α line radiation from nanosecond laser plasmas or ultrashort pulse laser-produced $K - \alpha$ inner-shell emission have been applied for backlighting [8] and dynamic diffraction [9,10] experiments. These laser-produced sources have been shown to fulfill the stringent requirements on photon numbers and bandwidth for spectrally resolved x-ray scattering measurements in single shot experiments [11–13]. This development has enabled quantitative *in situ* measurements of densities and temperatures with x-ray Thomson-scattering measurements [14].

In the first inelastic x-ray scattering measurements on dense plasmas, noncollective backscattering has been performed on isochorically heated solid Be targets [14]. These experiments demonstrated accurate temperature measurements from the spectral broadening of the Compton scattering feature that yields the electron velocity distribution. More recent experiments in forward scatter geometry have

observed collective plasmon features from electron density (Langmuir) oscillations yielding the electron density via the plasmon dispersion relation [15]. Recent applications of x-ray scattering techniques to probe shocked matter have succeeded in inferring dense matter properties from observations of bound-free [16–18] and forward scattering components [19,20].

In this Letter, we present the first observations of both the inelastic Compton and plasmon scattering spectra from shock-compressed dense matter that provide accurate measurements of temperature and density. Flat solid Be targets have been directly irradiated with a set of laser beams launching a strong shock wave that heats and compresses the target at pressures in the range of $20 < P < 35$ Mbar [16]. A second set of laser beams is delayed in time to produce 6.2 keV x rays that are scattered by the dense Be plasma as the shock traverses the target. This experiment accesses the noncollective and the collective scattering regime by observing the scattered radiation at two different scattering angles.

We find that the shock wave compression results in a Fermi-degenerate plasma where the noncollective spectra show a parabolic inelastic Compton scattering feature characteristic of a Fermi electron velocity distribution; the width directly provides a measure of the electron density and thus the Fermi energy. Moreover, the intensity ratio of elastic (Rayleigh) to inelastic (Compton) scattering allows the ion temperature to be inferred [21,22] indicating a high degree of degeneracy when assuming equilibration between electrons and ions in these high-density nanosecond laser experiments. Different from previous results in CH [16] the present experiment is dominated by contributions from free electrons, thus directly reflecting the electron density and Fermi energy. These findings agree with measurements performed in forward scattering that show collective plasmon oscillations. The plasmon frequency shift directly yields the electron density [23]; the

electron temperature is estimated from thermal corrections to the plasmon dispersion and damping. These findings agree with radiation-hydrodynamic modeling using the code LASNEX [24] indicating that x-ray Thomson scattering is a viable and accurate technique for providing critical experimental tests of basic concepts and assumptions of quantum statistical physics.

Figure 1 shows a schematic of the experiment that has been performed at the Omega laser facility [25]. Twelve laser beams smoothed with distributed phase plates (SG-4) overlap in ~ 1 mm diameter focal spot and directly illuminate a $250 \mu\text{m}$ thick Be foil; cf. Fig. 1(a). Each beam delivers up to about 480 J in a 1 ns square pulse. They are staggered in time reaching varying pressure conditions with 3–4 ns long constant drive and laser intensities of $10^{14} < I < 10^{15} \text{ W cm}^{-2}$; cf. Fig. 1(c). Radiation-hydrodynamic calculations indicate that these irradiation conditions launch a strong shock wave into the solid target

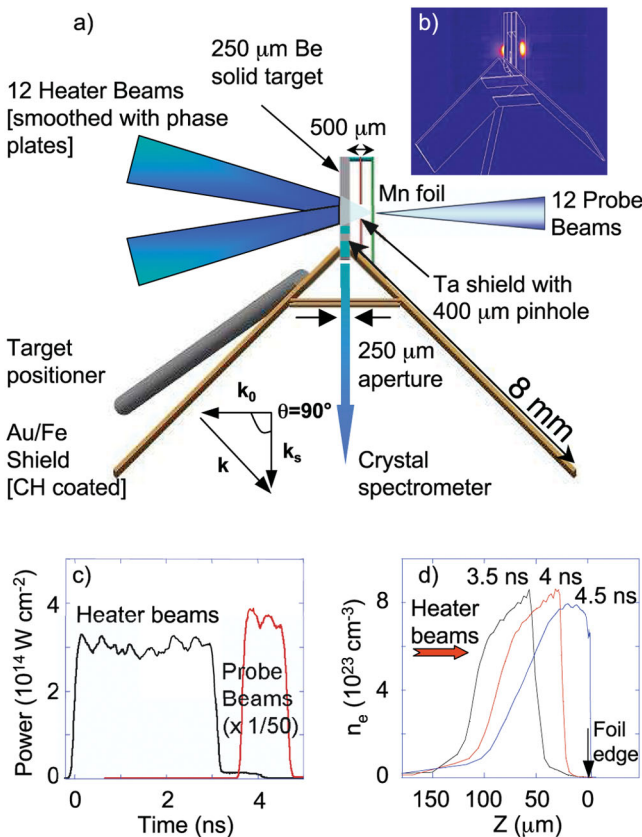


FIG. 1 (color). (a) Schematic of the experiment showing 12 heater beams that compress the Be foil and 12 delayed probe beams that produce $E = 6.2 \text{ keV}$ x rays. X-ray scattering spectra are observed in the downward direction with a gated crystal spectrometer. (b) A time-integrated x-ray image for $E > 2 \text{ keV}$ shows the emission produced by heater and probe beams. (c) Heater and probe beam intensity on target for a 3 ns-long drive. (d) Radiation-hydrodynamic calculations from LASNEX indicate a pressure of 30 Mbar and shock breakout at $t = 4.5 \text{ ns}$. The probe beams are delayed to probe conditions close to the time of shock breakout.

compressing the target homogeneously at pressures in the range of 20–35 Mbar.

At $t = 4.5 \text{ ns}$, when the shock has traversed the $250 \mu\text{m}$ thick foil, 12 delayed beams produce Mn He- α radiation to probe the dense plasma conditions. A $400 \mu\text{m}$ pinhole placed between the Mn and Be foils assures that only compressed Be has been intersected by the probe x rays. The calculations indicate that the target is compressed by a factor of 3 with fairly homogeneous electron density profiles with $7 \times 10^{23} < n_e < 8 \times 10^{23} \text{ cm}^{-3}$ for $I = 3 \times 10^{14} \text{ W cm}^{-2}$. The scattered photon fraction is determined by the product $n_e \sigma_{\text{TS}} \ell$, with σ_{TS} being the Thomson-scattering cross section and ℓ the length of the scattering volume; thus, scattering from the dense plasma region will dominate the scattering signal.

Figure 2 shows the scattering spectra for 90° and 25° scattering angle along with the Mn source spectrum. The measurements have been performed with a graphite crystal spectrometer coupled to a gated microchannel plate detector providing a temporal resolution of 100 ps. In contrast to x-ray scattering measurements on isochorically heated Be [14], a high-energy x-ray source with incident energy of $E_0 > 6 \text{ keV}$ is required to penetrate through compressed matter that is approaching $n_e = 10^{24} \text{ cm}^{-3}$. Although of sufficient x-ray energy, the present source has the disadvantage of consisting of two spectral features comprised by the 6.18 keV Mn He- α and the 6.15 keV intercombination lines [26]; cf. Fig. 2(d).

The Compton scattering spectrum measured at a scattering angle of $\theta = 90^\circ$ shows a parabolic spectrum downshifted in energy from the incident radiation by the Compton effect; the shift is determined by the Compton energy $E_C = \hbar^2 k^2 / 2m_e = 74 \text{ eV}$. Here, \mathbf{k} is the scattering vector with $k = 4\pi(E_0/hc) \sin(\theta/2) = 4.4 \text{ \AA}^{-1}$ indicating noncollective scattering with a scattering parameter $\alpha = 1/k\lambda_S = 0.5$ and λ_S being the screening length [27]. The Compton scattering spectrum directly reflects the electron distribution function; for a Fermi-degenerate system the width of the Compton spectrum yields the Fermi energy,

$$E_F = \frac{\hbar^2}{2m_e} (3\pi^2 n_e)^{2/3}. \quad (1)$$

The fit of the experimental data using the theoretical form factor of Refs. [27,28] shows that the width of the Compton feature is sensitive to the electron density. The free electron feature is derived with the random phase approximation and the ion peak is fitted consistent with results from density-functional theory. The fit takes into account the detailed spectral features of the Mn source spectrum as well as instrument broadening. In addition, the small level of continuum radiation has been subtracted and corrections due to the spectral response of the spectrometer have been included. Figure 2(a) compares the data to calculations with varying electron density ranging from noncompressed Be with $n_e = 3 \times 10^{23} \text{ cm}^{-3}$ to more than fourfold compression with $n_e = 1.2 \times 10^{24} \text{ cm}^{-3}$.

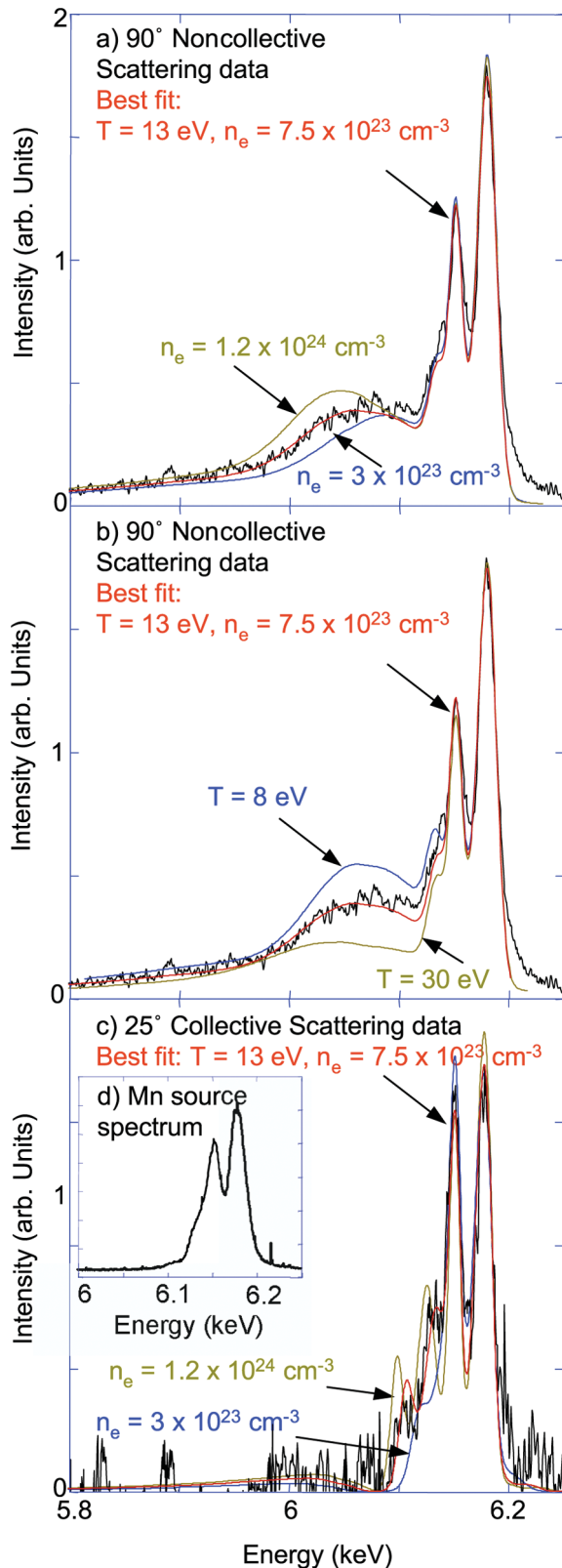


FIG. 2 (color). (a) X-ray scattering data for 90° scattering angle are shown along with theoretical spectra for various electron densities. (b) Same as in (a) for various ion temperatures. (c) X-ray scattering data for 25° scattering angle are shown along with theoretical spectra for various electron densities. (d) The inset shows the Mn x-ray probe spectrum.

Because of the small noise levels, the data determine the electron density to be $n_e = 7.5 \times 10^{23} \text{ cm}^{-3}$ with the corresponding Fermi energy of $E_F = 30 \text{ eV}$ with error bars of $\pm 7\%$ in density.

Relating the Fermi energy with the electron density via Eq. (1) is motivated by the distribution function inferred from fitting the experimental Compton scattering data [11]. Bound-free transitions have been included using hydrogenic wave functions. The main effect is a high-energy tail with shifts $>100 \text{ eV}$ as apparent in the data and in the fits. The ionization state has been set to $Z = 2$ in agreement with radiation-hydrodynamic modeling. The shape of the Compton feature is consistent with this value with an estimated accuracy of $\pm 25\%$; the latter takes into account density that the plasmons agree with the Compton scattering data.

The intensity of the elastic scattering feature indicates a temperature significantly lower than the Fermi energy. In the present conditions with large scattering vector, the contribution from electrons in the screening cloud is negligible, and the strength of the elastic scattering feature is approaching $f^2 S_{ii}(k, \omega)$ [29]. The ion form factor $f(k)$ is a measure of the number of bound electrons and $S_{ii}(k, \omega)$ is the ion-ion density correlation function. Thus, with absolute calibration provided by the measured strength of the inelastic Compton scattering feature and knowledge of the electron density, $S_{ii}(k, \omega)$ is determined absolutely from the experimental scattering data. Consequently, the ion temperature can be inferred from the intensity ratio of elastic to inelastic scattering.

Figure 2(b) indicates that this procedure is sensitive to variations in temperature leading to error bars of 10% for conditions with well-known structure factors. For the k vector of Fig. 2(b), we employ the previously tested theory of Ref. [27] leading to an ion temperature of $T_i = 13 \text{ eV}$. These scattering spectra show a significant difference from cold Be as shown in, e.g., Ref. [14], indicating sensitivity to density and temperature. Densities and temperatures inferred in this way from the noncollective scattering data are consistent with results obtained in forward scattering.

Figure 2(c) shows the experimental scattering data measured at 25° scattering angle accessing the collective scattering regime with $\alpha = 1.56$ and $k = 1.36 \text{ \AA}^{-1}$. In contrast to noncollective scattering, the broad inelastic Compton scattering feature is replaced with two small plasmon features, that are shifted in energy by $\sim 40 \text{ eV}$ from the incident x-ray probe features. In this case, the frequency shift due to the Compton effect is small of order 7 eV and the frequency shift of the plasmon is determined by the frequency of plasma oscillations. The theoretical fit to the measured spectrum indicates the same densities and temperatures as obtained for noncollective scattering; comparing the scattering data with spectra calculated at various densities indicates that the frequency shift of the plasmon provides an accurate measure of the electron density of $n_e = 7.5 \times 10^{23} \text{ cm}^{-3}$ with error bars of $\pm 6\%$. Con-

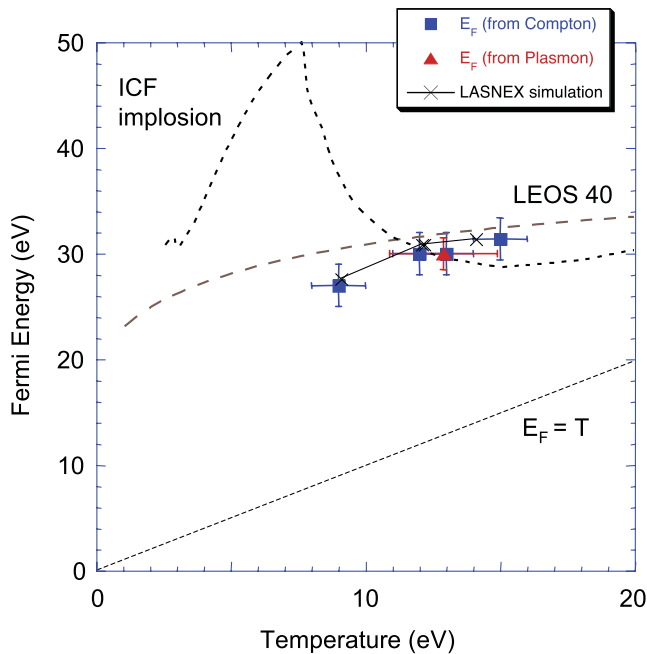


FIG. 3 (color). Fermi energies inferred from the measured densities from the Compton and plasmon scattering data are shown versus temperature. A high level of degeneracy is found close to predictions from LASNEX (solid curve) and the LEOS data table (long dashed curve). Also shown are the trajectory of Be in ICF implosion modeling (dashed curve) together with the curve $E_F = T$ (short dashed curve).

versely, using the electron density from the 90° scattering data, we obtain an estimate of $T_e = 13 \pm 3$ eV for the electron temperature from the thermal corrections to the plasmon dispersion. Moreover, the fit shown in Fig. 2(c) accounts for damping processes of plasmons by Landau and collisional damping [30] as well as the detailed balance relation indicating that the density and temperatures inferred in this way provide a width and intensity of the plasmon consistent with the measurements.

In shots at various laser intensities, we changed the shock properties, i.e., the density and the temperature. The resulting values for T and the Fermi energy according Eq. (1) are summarized in Fig. 3. The experiments demonstrate a direct measurement of the degeneracy and adiabat in these single-shocked foils. The direct comparison with LASNEX simulations that use the LEOS equation of state [31] shows excellent agreement with the data. The simulations indicate slightly lower compression than the Hugoniot data predicted by LEOS by accounting for x-ray preheat and averaging over the densities in the shocked region; cf. Fig. 1(d). The agreement with LASNEX indicates that the conditions at low drive show observable effects of gradients. However, the data measured at higher drive agree well with both LASNEX and LEOS.

Also shown are calculations of the conditions predicted for ICF experiments during the implosion phase. These calculations use a Be ablator and predict ignition and gain

employing a 1.2 MJ laser drive on the National Ignition Facility. The present experiment shows that these conditions are accessible by x-ray Thomson scattering that motivate a direct measurement of the degeneracy during the assembly of the thermonuclear fuel.

In summary, we have demonstrated collective and non-collective x-ray Thomson-scattering techniques in shock-compressed matter conditions. These measurements have provided accurate data on density and temperature in close agreement with calculations. This method allows application to a number of dense matter questions including future applications to measure degeneracy and adiabat, e.g., in ICF and high energy density physics studies.

This work performed under the auspices of the U.S. Department of Energy by Lawrence Livermore National Laboratory under Contract No. DE-AC52-07NA27344. Work was also supported by the National Laboratory User Facility, Laboratory Directed Research and Development Grants No. 08-ERI-002 and No. 08-LW-004, by the Helmholtz association (VH-VI-104) and by the Deutsche Forschungsgemeinschaft (SFB 652).

-
- [1] V.E. Fortov *et al.*, Phys. Rev. Lett. **99**, 185001 (2007).
 - [2] S. A. Bonev *et al.*, Nature (London) **431**, 669 (2004).
 - [3] G. W. Collins *et al.*, Science **281**, 1178 (1998).
 - [4] J. D. Lindl *et al.*, Phys. Plasmas **11**, 339 (2004).
 - [5] R. L. McCrory *et al.*, Phys. Plasmas **15**, 055503 (2008).
 - [6] O. L. Landen *et al.*, J. Quant. Spectrosc. Radiat. Transfer **71**, 465 (2001).
 - [7] R. W. Lee *et al.*, J. Opt. Soc. Am. B **20**, 770 (2003).
 - [8] B. A. Hammel *et al.*, Phys. Fluids B **5**, 2259 (1993).
 - [9] H. J. Lee *et al.*, Phys. Rev. B **77**, 132301 (2008).
 - [10] D. Riley *et al.*, Phys. Rev. Lett. **84**, 1704 (2000).
 - [11] O. L. Landen *et al.* Rev. Sci. Instrum. **72**, 709 (2001).
 - [12] M. K. Urry *et al.*, J. Quant. Spectrosc. Radiat. Transfer **99**, 636 (2006).
 - [13] A. L. Kritcher *et al.*, High Energy Density Phys. **3**, 156 (2007).
 - [14] S. H. Glenzer *et al.*, Phys. Rev. Lett. **90**, 175002 (2003).
 - [15] S. H. Glenzer *et al.*, Phys. Rev. Lett. **98**, 065002 (2007).
 - [16] H. Sawada *et al.*, Phys. Plasmas **14**, 122703 (2007).
 - [17] A. Ravasio *et al.*, Phys. Rev. Lett. **99**, 135006 (2007).
 - [18] D. Riley *et al.*, Laser Part. Beams **25**, 465 (2007).
 - [19] E. G. Saiz *et al.*, Nature Phys. **4**, 940 (2008).
 - [20] A. L. Kritcher *et al.*, Science **322**, 69 (2008).
 - [21] V. Schwarz *et al.*, Contrib. Plasma Phys. **47**, 324 (2007).
 - [22] K. Wünsch *et al.*, Phys. Rev. E **77**, 056404 (2008).
 - [23] R. Thiele *et al.* Phys. Rev. E **78**, 026411 (2008).
 - [24] G. B. Zimmerman and W. L. Kruer, Comments Plasma Phys. Controlled Fusion **2**, 51 (1975).
 - [25] J. M. Soures *et al.*, Fusion Technol. **30**, 492 (1996).
 - [26] D. B. Sinars *et al.*, Rev. Sci. Instrum. **77**, 10E309 (2006).
 - [27] G. Gregori *et al.*, Phys. Rev. E **67**, 026412 (2003).
 - [28] G. Gregori *et al.*, Phys. Rev. E **74**, 026402 (2006).
 - [29] J. Chihara, J. Phys. Condens. Matter **12**, 231 (2000).
 - [30] R. Redmer *et al.*, IEEE Trans. Plasma Sci. **33**, 77 (2005).
 - [31] R. M. More *et al.*, Phys. Fluids **31**, 3059 (1988).